STARS

Faculty Bibliography 2010s

Faculty Bibliography

1-1-2013

Shockwave based nonlinear optical manipulation in densely scattering opaque suspensions

Elad Greenfield

Jonathan Nemirovsky

Ramy El-Ganainy
University of Central Florida

Demetri N. Christodoulides
University of Central Florida

Mordechai Segev

Find similar works at: https://stars.library.ucf.edu/facultybib2010

University of Central Florida Libraries http://library.ucf.edu

Recommended Citation

Greenfield, Elad; Nemirovsky, Jonathan; El-Ganainy, Ramy; Christodoulides, Demetri N.; and Segev, Mordechai, "Shockwave based nonlinear optical manipulation in densely scattering opaque suspensions" (2013). *Faculty Bibliography 2010s*. 4053.
https://stars.library.ucf.edu/facultybib2010/4053

University of Central Florida

STARS

Showcase of Text, Archives, Research & Scholarship

Shockwave based nonlinear optical manipulation in densely scattering opaque suspensions

Elad Greenfield,[1] Jonathan Nemirovsky,[1] Ramy El-Ganainy,[2] Demetri N. Christodoulides,[2] and Mordechai Segev[1*]

[1]*Physics Department and Solid State Institute, Technion, Haifa 32000, Israel*
[2]*CREOL - College of Optics & Photonics, University of Central Florida, Orlando, Florida 32816, USA*
[*]*msegev@tx.technion.ac.il*

Abstract: Optical manipulation of particulate-loaded, highly scattering (opaque) suspensions is considered impossible. Here we demonstrate theoretically and experimentally optical manipulation of the local properties of such opaque suspensions. We show that the optical forces exerted by multiply-scattered light give rise to dense shock fronts of particle concentration, propagating deep inside the opaque suspensions, where the optical field is completely diffuse. We exploit these waves to demonstrate a plethora of optofluidic manipulations, ranging from optical transport and concentration of large populations of nanoparticles, to light-induced 'writing' of concentrated spots in the suspensions and light-induced phase-transition from suspension to gel in localized volumes inside the fluids.

©2013 Optical Society of America

OCIS codes: (070.7345) Wave propagation; (170.5270) Photon density waves; (290.4210) Multiple scattering.

References and links:

1. Y. Fainman, *Optofluidics: Fundamentals, Fevices, and Applications*, (McGraw-Hill, 2010).
2. D. Psaltis, S. R. Quake, and C. H. Yang, "Developing optofluidic technology through the fusion of microfluidics and optics," Nature **442**(7101), 381–386 (2006).
3. U. Levy and R. Shamai, "Tunable optofluidic devices," Microfluid. Nanofluid. **4**(1-2), 97–105 (2008).
4. S. Kim, A. M. Streets, R. R. Lin, S. R. Quake, S. Weiss, and D. S. Majumdar, "High-throughput single-molecule optofluidic analysis," Nat. Methods **8**(3), 242–245 (2011).
5. A. E. Vasdekis, E. A. Scott, C. P. O'Neil, D. Psaltis, and J. A. Hubbell, "Precision intracellular delivery based on optofluidic polymersome rupture," ACS Nano **6**(9), 7850–7857 (2012).
6. A. Ashkin, *Optical Trapping and Manipulation of Neutral Particles Using Lasers*. (World Scientific, 2006).
7. S. L. Jacques and B. W. Pogue, "Tutorial on diffuse light transport," J. Biomed. Opt. **13**(4), 041302 (2008).
8. L. V. Wang and H. I. Wu, *Biomedical Optics: Principles and Imaging*. (Wiley-Interscience, 2007).
9. J. Mewis and N. J. Wagner, *Colloidal Suspension Rheology*, (Cambridge University Press, 2012).
10. I. M. Vellekoop and A. P. Mosk, "Focusing coherent light through opaque strongly scattering media," Opt. Lett. **32**(16), 2309–2311 (2007).
11. I. M. Vellekoop, A. Langendijk, and A. P. Mosk, "Exploiting disorder for perfect focusing," Nat. Photonics **4**, 320–322 (2010).
12. O. Katz, E. Small, Y. Bromberg, and Y. Silberberg, "Focusing and compression of ultrashort pulses through scattering media," Nat. Photonics **5**(6), 372–377 (2011).
13. O. Katz, E. Small, and Y. Silberberg, "Looking around corners and through thin turbid layers in real time with scattered incoherent light," Nat. Photonics **6**, 549–553 (2012).
14. T. Cizmar, M. Mazilu, and K. Dholakia, "In situ wavefront correction and its application to micromanipulation," Nat. Photonics **4**, 388–394 (2010).
15. P. L. Sachdev, *Nonlinear Diffusive Waves*, (Cambridge University Press, 1987).
16. A. Ashkin, J. M. Dziedzic, and P. W. Smith, "Continuous-wave self-focusing and self-trapping of light in artificial Kerr media," Opt. Lett. **7**(6), 276–278 (1982).
17. V. E. Yashin, S. A. Chizhov, R. L. Sabirov, T. V. Starchikova, N. V. Vysotina, N. N. Rozanov, V. E. Semenov, V. A. Smirnov, and S. V. Fedorov, "Formation of soliton-like light beams in an aqueous suspension of polystyrene particles," Opt. Spectrosc. **98**(3), 466–469 (2005).
18. C. Stockbridge, Y. Lu, J. Moore, S. Hoffman, R. Paxman, K. Toussaint, and T. Bifano, "Focusing through dynamic scattering media," Opt. Express **20**(14), 15086–15092 (2012).
19. M. Anyfantakis, A. Koniger, S. Pispas, W. Kohler, H. J. Butt, B. Loppinet, and G. Fytas, "Versatile light actuated matter manipulation in transparent non-dilute polymer solutions," Soft Matter **8**(8), 2382–2384 (2012).

20. M. Anyfantakis, B. Loppinet, G. Fytas, and S. Pispas, "Optical spatial solitons and modulation instabilities in transparent entangled polymer solutions," Opt. Lett. **33**(23), 2839–2841 (2008).
21. R. Sigel, G. Fytas, N. Vainos, S. Pispas, and N. Hadjichristidis, "Pattern formation in homogeneous polymer solutions induced by a continuous-wave visible laser," Science **297**(5578), 67–70 (2002).
22. R. Wunenburger, B. Issenmann, E. Brasselet, C. Loussert, V. Hourtane, and J. P. Delville, "Fluid flows driven by light scattering," J. Fluid Mech. **666**, 273–307 (2011).
23. C. Conti, N. Ghofraniha, G. Ruocco, and S. Trillo, "Laser beam filamentation in fractal aggregates," Phys. Rev. Lett. **97**(12), 123903 (2006).
24. C. Conti and E. DelRe, "Optical supercavitation in soft Matter," Phys. Rev. Lett. **105**(11), 118301 (2010).
25. E. Greenfield, C. Rotschild, A. Szameit, J. Nemirovsky, R. El-Ganainy, D. N. Christodoulides, M. Saraf, E. Lifshitz, and M. Segev, "Light-induced self-synchronizing flow patterns," New J. Phys. **13**(5), 053021 (2011).
26. Y. Lamhot, A. Barak, O. Peleg, and M. Segev, "Self-trapping of optical beams through thermophoresis," Phys. Rev. Lett. **105**(16), 163906 (2010).
27. Y. Lamhot, A. Barak, C. Rotschild, M. Segev, M. Saraf, E. Lifshitz, A. Marmur, R. El-Ganainy, and D. N. Christodoulides, "Optical control of thermocapillary effects in complex nanofluids," Phys. Rev. Lett. **103**(26), 264503 (2009).
28. K. M. Douglass, S. Sukhov, and A. Dogariu, "Superdiffusion in optically controlled active media," Nat. Photonics **6**(12), 834–837 (2012).
29. Y. L. Guo, A. Morozov, D. Schneider, J. W. Chung, C. Zhang, M. Waldmann, N. Yao, G. Fytas, C. B. Arnold, and R. D. Priestley, "Ultrastable nanostructured polymer glasses," Nat. Mater. **11**(4), 337–343 (2012).
30. C. F. Bohren and D. R. Huffman, *Absorption and Scattering of Light by Small Particles*, (Wiley-Interscience, 1983).
31. T. Inagaki, E. T. Arakawa, R. N. Hamm, and M. W. Williams, "Optical-properties of polystyrene from near-Infrared to X-Ray region and convergence of optical sum-rules," Phys. Rev. B **15**(6), 3243–3253 (1977).

1. Introduction

Optofluidics, the science of light interaction with fluids, presents a host of attractive and versatile alternatives to traditional technologies [1,2]. The understanding of fundamental light-fluid interactions is now rapidly growing - already giving rise to valuable technological advancements: tunable wavelength optofluidic lasers [3], optofluidic single-molecule analysis [4], and optofluidic Intracellular delivery [5], are only a few examples. Indeed, optical manipulation has now become a common tool for a variety of applications [1,6]. It completely relies on the ability to tailor the optical fields and forces inside the volume of the fluid. Nowadays, this is routinely done in dilute suspensions, within which designing the optical fields can be done at sub-wavelength accuracy. However, densely-packed suspensions scatter the light so heavily that such suspensions are opaque: the light diffuses, losing its directionality and localization [7,8]. Indeed, optical manipulation in strongly-scattering suspensions is considered impossible: the optical field cannot be externally tailored inside such suspensions, thus rendering these suspensions largely inaccessible to optical manipulation. This poses a severe limitation to optofluidics: Densely-packed suspensions of particles are extremely important in almost every aspect of daily life. They range from biological suspensions such as blood, plasma, natural minerals, milk and foods, to synthetic nanoparticle-based drugs, polluted fluids, inks and paints [9]. The ability to manipulate the local properties of the fluid in small volumes within such suspensions would therefore be very important, especially if such manipulation can be done with light. In a related context, recent progress in wavefront-correction methods did allow focusing light behind a scattering medium [10–13], which holds potential for revolutionizing biomedical imaging. However, these techniques cannot work for optical manipulation in heavily-scattering fluids, mainly because the wavefront aberration introduced by fluids evolves quickly in time due to Brownian or optical-force induced motion of the particles inside the fluids. Indeed, thus far optical manipulation with these methods has been largely unstudied, and the few attempts were strictly limited to weakly-scattering, time-stationary solid medium [14], where the optical thickness is much smaller than the photon transport-mean-free-path.

Here, we present the first experiments and theory on optical manipulation of the local properties of dense, particulate-loaded, highly-scattering (opaque) suspensions of nanoparticles. We show that multiply-scattered light can give rise to shock fronts of dense particle concentration, propagating deep inside the opaque suspensions. These waves are

generated by the interplay between the optical gradient force and radiation pressure [6], while no thermal effects are involved. We exploit these waves to yield a plethora of new ways to manipulate the local properties of opaque fluids using only diffuse light. We demonstrate optical transport and concentration of large populations of nanoparticles deep inside dense opaque fluids, clearing of localized volumes of opaque solutions from particles, and generation of directional filaments of particles, propagating up to 15 photon transport mean free paths [7] (MFPs) into the suspensions. Last but not least, we observe light-induced phase transitions in a localized volume inside a microfluidic channel. In this scenario, light concentrates the particles in a micrometer-scale volume inside the suspension. When the concentration exceeds a critical value for a suspension to gel phase transition, a small gel 'ball' forms deep inside the suspension. Using optical forces, we manipulate such gel balls deep inside the dense fluid by remote, positioning them at preselected locations.

2. Theoretical

The phenomena described here are observed when intense light is focused into optically dense, light-scattering suspensions of nanoparticles. Traditionally, when a beam of light is launched into non-absorbing light-scattering media, its propagation deep inside the suspension is described by a linear diffusion equation [7,8],

$$\frac{\partial \varphi_{ph}}{\partial t} = \vec{\nabla} \cdot \left(D_{ph} \vec{\nabla} \varphi_{ph} \right) \tag{1}$$

with $\varphi_{ph}(r,t)$ being the density of photons, and r, t the space and time coordinates, respectively. According to Eq. (1), a directional beam of light entering the medium diffuses in all directions, with photon transport MFP acting as the reciprocal of D_{ph}, where D_{ph} is the photon diffusion coefficient, which is a constant for an homogeneous suspension. As a rule of thumb, the diffusion approximation is in good agreement with exact (Monte–Carlo) simulations of light transport in scattering media, for light that has traveled a distance of more than two photon MFPs from the light source into the scattering media [7]. In the framework described by Eq. (1), the medium itself is stationary, being unaffected by the light that scatters in it, since Eq. (1) neglects the influence of optical forces on the scattering medium.

The 'stationary medium' approximation holds well in a solid diffuser, where the scattering centers are stationary. But when an intense beam of light illuminates a liquid-particulate mixture, neglecting the forces the scattered light exerts on the scattering particles no longer describes the physical reality. The particles in the suspension indeed scatter the light, but at the same time the scattered light exerts radiation pressure and optical gradient forces on the particles themselves. If the light is sufficiently intense, these optical forces can easily overcome any other forces acting on the particles, such as Brownian forces, inter-particle interactions, and gravity. The optical forces acting on the particles, moving them around, and in turn the physical properties of the medium itself evolve in space and time. For example, if light thrusts the scattering particles out of some volume of fluid, the local particle concentration, density and the photon diffusion coefficient in this volume will change accordingly. In this case, D_{ph} becomes a function of space and time, whose evolution is dictated by the nonlinear dynamics of light and fluid. Once D_{ph} is no longer a constant, counter to intuition- the solutions to the photon diffusion equation (Eq. (1)), do not have to be diffusive at all, and richer dynamics may arise. Hence, when dealing with 'liquid optical diffusers', it is essential to incorporate optical forces into the framework. The new dynamics that arise are in the heart of the current work.

To account for the effects of optical forces, we introduce a transport equation for the density of scattering particles in the suspension, $\rho(r,t)$, under the influence of optical forces,

and solve this equation along with Eq. (1). Leaving the mathematical details of this derivation to Appendix A, the coupling between the two equations gives rise to a single, nonlinear Burgers-type equation [15] for the particle concentration in the medium:

$$\frac{\partial \rho}{\partial \tau} = A \frac{\partial^2 \rho}{\partial x^2} - B\rho \frac{\partial \rho}{\partial x}, \tag{2}$$

where A and B are constants that depend on the parameters of the problem (appearing explicitly in Appendix A), and the coordinates τ and x are the time and space coordinates in a frame of reference moving with the drag velocity of the particles. For simplicity, we analyze here a one-dimensional problem.

Importantly, the nonlinearity of Eq. (2) is an inherent property of the interaction of light with light-scattering suspensions. The Burgers equation arises quite often in nonlinear dispersive wave-supporting systems, when the velocity of a 1D physical quantity depends on the value of that quantity (that is: the local and instantaneous velocity of the particles with local concentration $\rho(x,t)$ in Eq. (2) is $B\rho(x,t)$). But the underlying physics can take many different forms. In our case, the nonlinearity in Eq. (2) stems from the optical gradient force acting on the particles which at the same time scatter the optical field diffusively. This nonlinearity is not to be confused, for examples, with an optical nonlinearity of the dielectric properties of the materials involved, or due to their dependence on temperature (Eq. (2) neglects thermal effects, assuming that the light does not heat up the nano-suspensions, as verified later on in the experiments- see details in Appendix B).

The Burgers equation (of the form of Eq. (2)) is well known to support shock wave solutions. Here, an intense beam of light illuminating a dense scattering suspension generates intense particle-density shock waves that propagate throughout the volume of the suspension. The solution of the one-dimensional Burgers equation (Eq. (2) predicts the formation of sharp shock-fronts in a reference frame moving at the drag velocity, while causing depletion in the particles' concentration in the immediate region trailing the shock-fronts. This idea has served as the initial motivation for our experiments. As we show below, the experiments indeed present shock waves, but the intriguing physics involved is far more complex, and entails a variety of new phenomena.

3. Experimental

In our experiments, we use glass micro-channels filled with a dense, strongly scattering, 'milky' appearing silica (or polystyrene) colloidal suspension (Fig. 1(a). Three examples of such suspensions are, for instance, (10% w/v)- 150 nm and 320 nm diameter silica spheres, and 100 nm diameter Polystyrene spheres- suspended in pure DI water. These suspensions are opaque for visible light propagating in the micro-channel cells, even in their narrowest dimension – the thickness of the channel (250μm) is shown in Fig. 1(a). Visible light entering the suspension diffuses in all directions, as depicted in Fig. 1(b): a green laser beam entering a suspension-filled microfluidic channel from the left (marked with a green arrow) diffuses evenly in all directions, while the portion of light which remains directional decays rapidly in the forward direction. In our suspensions, absorption of light at the visible range is negligible over distances much larger than those in our experiments. Consequently, thermal effects were completely absent in our experiments, as we ascertain using a commercial thermal camera (the details of these experiments are in the Appendix B of the article). The schematic of the experimental apparatus is presented in Fig. 1(c). The light is coupled into the micro-channel through a multimode fiber (mode diameter ~10μm) inserted into the middle of the channel, to avoid effects associated with possible reflections from the entrance wall of the channel and optical aberrations associated with the liquid-air surface meniscus. Light from a CW green laser ($\lambda = 532nm$) is coupled into the fiber, entering the dense suspension through the fiber. We emphasize that the fiber coupling is used just to obtain clean and stable results, but the

physical effects presented here do not arise from the fiber. To verify this, we repeat the experiments without the fiber, with a laser beam entering from air and directly focused into the suspension. The effects presented below are observed also without the fiber, but their stability and controllability are severely hindered by surface effects at the suspension-air interface. Finally, to experimentally observe physical phenomena occurring deep inside heavy scattering regions we have developed an additional experimental apparatus for data acquisition. Obviously, the dynamics within the fluid cannot be resolved from the intense scattered light, such as that presented in Fig. 1(b). To observe the dynamics within the fluid, the channel is viewed from the side with a near-infrared (NIR) imaging apparatus. For NIR radiation ($\lambda = 980 - 1064 nm$), the scattering diminishes, and the photon MFP (400~1400μm) is larger than the channel cross sectional dimension (250μm). Since the NIR light does not scatter substantially, it can be used for imaging. The resulting image is a shadowgram of the particle distribution in the channel. The NIR imaging system includes a fast (200 frames per second (fps)) area-scan camera, making it possible to view the dynamics within the fluid in real time, and an optical filter to block the scattered green light. In our experiments we use glass microfluidic channels with two different sizes: 250μm x 250μm x 10mm, and 250μm x 1000μm x 10mm, hence on referred to as the 'thin' and 'thick' channels respectively . A typical image of the thinner channel with the fiber inserted into it, as obtained with the NIR system, is presented in Fig. 1(d).
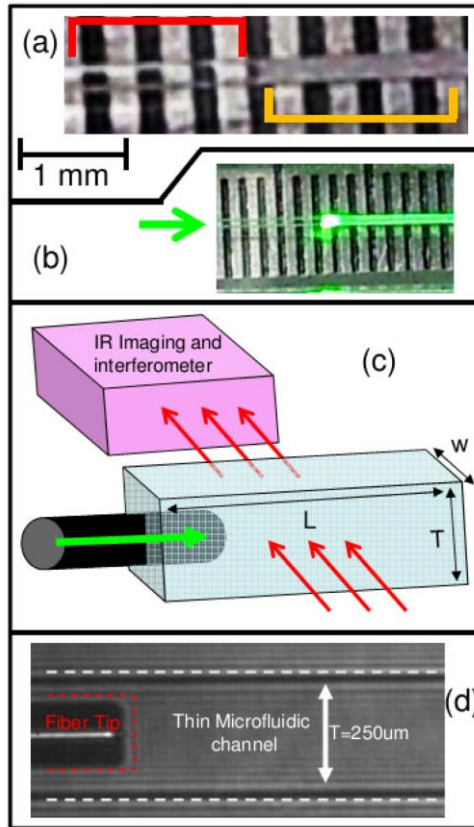
Fig. 1. Experimental setup for generating and observing light-induced shock-waves of nanoparticle-concentration in dense opaque fluids. (a) The thin glass micro-channel presented on top of a ruler. The channel is partially filled with light-diffusing suspension (10%, 320nm diameter glass spheres). The filled and unfilled regions of the channel are marked in yellow and red respectively. The suspension is opaque: the ruler marks below the suspension-filled channel are not visible, whereas the marks are easily visible through the empty region of the channel (b) A green laser beam enters the micro-channel from the left (green arrow). When the light enters the suspension, it diffuses in all directions. (c) Experimental setup: the glass micro-channel, and a multimode optical fiber to couple the light directly into the channel. The dynamics within the fluid is probed with a near-infra-red (NIR) imaging system, supplemented by an interferometer and a fast camera. (d) Typical image obtained with the NIR imaging system, showing the channel from the side, and the fiber tip inserted into it.

In a typical experiment, we inject 1-3 Watts of laser-power into the fluid through the fiber. When the light illuminates the dense suspension, it scatters from the particles in all directions (Fig. 1(b)). Looking at the dazzling green scattered light (Fig. 1(b)), one does not intuitively expect any ordered or localized effects to occur in the diffusive medium. Nevertheless, when we view the nanoparticle concentration, as it evolves in real-time, with the NIR imaging system, we observe that *the scattered light induces localized, directional spearhead shaped, concentration shock-fronts* propagating distances of several photon transport MFPs into the fluid, in accordance with the predictions of Eq. (2). The nanoparticles are pushed in the propagation direction and radially outward, forming concentration fronts resembling a 'spearhead' of concentrated particles propagating along the channel (to the right, in Figs. 1, 2). This 'spearhead' geometry is visible whether the wave is propagating inside the thick microfluidic channel, which limits the shocks propagation to two dimensions (Fig. 2(b)), or whether the wave propagates in the thin microfluidic channel, which limits the shock's

propagation to one dimension (Fig. 2(a)). A channel can be considered 'thin' if in the process of the light-induced forced 'jamming' the particles at the walls of the channel and then the fluid flow them back into the laser beam- all within a time scale comparable to the timescale of the propagation of the shock along the channel. On the other hand, a channel can then be considered 'thick' if its width is comparable to the distance for which the shock wave propagates in the channel before decaying (~1mm in Fig. 2). The evolution of the shock in time is readily visible in "Media 1" and "Media 2" which are available online. As shown in Fig. 2, these shocks concentrate both matter and light: it concentrates large populations of nanoparticles in distinct, localized volumes, up to 15 MFPs deep inside the scattering suspensions. This is entirely counterintuitive, since this deep in the suspension one would expect that light should be completely diffusive, not giving rise to such spatially localized effects.

We measure the profile of the shock front with an interferometric setup. Leaving the technical details to Appendix C, this setup facilitates direct measurement of the refractive index-change as the shock-front sweeps a preselected position in the suspension (the green 'X' marks in Fig. 2(b)), simultaneously with 'conventional' fast imaging of the dynamics. From this data, it is straightforward to deduce the profile of nanoparticle concentration at the shock-front. Figure 2(c) shows this data for four power levels of the input beam. In this case, the concentration of the nanoparticles in the shock-fronts is up to 55% higher than the concentration in the bulk suspension. In absolute numbers, the concentration at the peak of the shock front is up to 15.5% (w/v), compared with the initial 10%, uniformly distributed when the light beam is off.

The optical forces giving rise to the nonlinear effects manifested in Eq. (2) result in a tendency of the wave-fronts to pick-up ('sweep') the nanoparticles they encounter on their way. Accordingly, we directly observe light-induced transparency and optical clearing of localized volumes in the suspension from particles: the outwards-moving shock fronts clear the nanoparticles away from those regions through which the shocks have already propagated. By measuring the particle concentration in the shock-cleared regions trailing the shock-front (Fig. 2(c)), we find that the particles' concentration is down to (absolute) 3% in those regions – a 70% reduction from the initial 10% uniform concentration in the bulk. The Burgers equation (Eq. (2) describes the dynamics in a frame of reference moving with the drag velocity, v_{drag}, and its solution predicts that the region already affected by the shock $x < v_{drag} \cdot t$, t being the time from laser turn-on, is completely clear of particles. Experimentally, the observed particle clearing effect is not as sharp as Eq. (2) predicts, because the experimental geometry is not strictly 1D, and particles can still flow back to the cleared region. If the laser light is applied continuously to our system, the light induces transparency in the scattering medium: additional light entering the particulate-cleared volume can propagate ballistically instead of diffusively, and thus can be focused much deeper into these suspensions, thereby self-increasing the photon MFP considerably. Figure 2(d) presents the results of a numerical simulation of the 1D model for the light-fluid dynamics. Comparing the observed shocks in Fig. 2(c) to the theoretical prediction in Fig. 2(d) shows good qualitative agreement: the numerical simulation of the light-fluid dynamics under the action of optical forces mimics many of the observed effects, such as dense propagating matter shocks, and particle clearing.
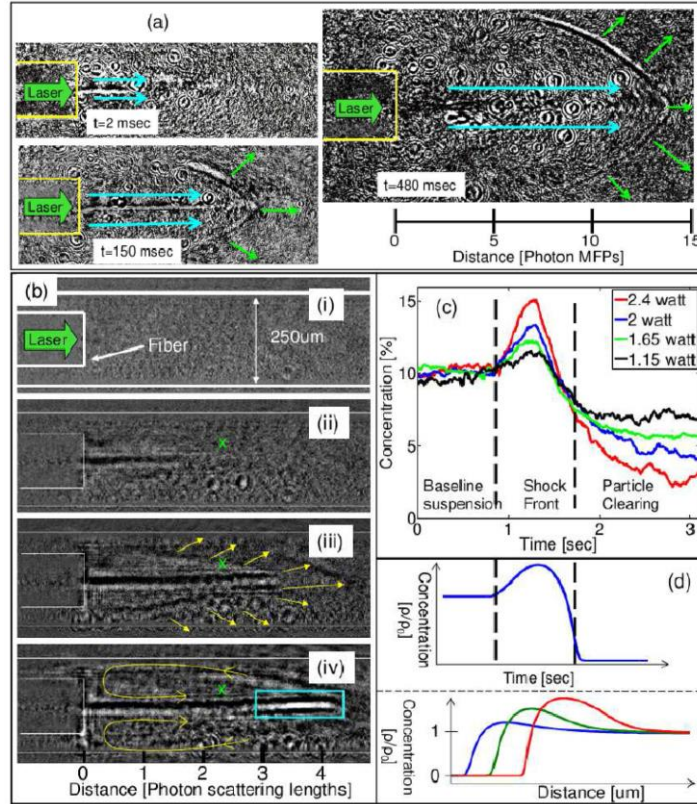
Fig. 2. Experimental observation of light-induced concentration shock-waves and optical clearing within opaque fluids. (a) The thick channel is filled with dense colloidal suspension. The laser delivers 2 watts of green light into the channel through the fiber (fiber contour marked in yellow). A dense spearhead-shaped nanoparticle wave-front is propagating to the right and radially outward, penetrating up to 15 photon transport MFP's into the suspension. The wave is shown at three successive times. The spear-shape is highlighted with green arrows indicating vectors normal to the wave-front. A filament (between the two cyan arrows) of high particle concentration develops along the channel, guiding light deep into the suspension. The evolution of the wave is presented in 'Media 1' available online. (b) The thin channel is filled with dense colloidal suspension and the laser delivers ~2.3 watts of green light into the channel through the fiber (fiber and channel contours are marked in white). (*i-iv*) The evolution of a dense nanoparticle wave-front, propagating in a 'spearhead-like' geometry, shown at four successive times. The spearhead-like propagation is highlighted in (*iii*) with yellow arrows indicating vectors normal to the wave-front. At the same time, nanoparticles accumulate at the spearhead tip (enclosed with a cyan rectangle in (*iv*)). The flow pattern supporting the formation of the particle accumulation is indicated by yellow arrows. The evolution of the wave is presented in 'Media 2' available online. (c) Experimentally measured light-induced concentration waves, exhibiting a steep concentration shock-front, and a particle-cleared region trailing the shock-front. The shock profiles display waves generated at four different laser power levels. The 'baseline' concentration in the undisturbed suspension is 10%. As the shock-front passes through the monitored position in the suspension (marked by green X in a-*iii*) we measure a steep concentration increase, up to 15.5 (55% higher than the baseline), and increasing with optical power. The shock sweeps the particles with it, effectively clearing the area through which the shock has passed. After the shock has passed, the concentration is up to 70% lower than the baseline (as low as 3% concentration). These measurements are obtained with an interferometric apparatus whose details are in Appendix C. (d) Numerical simulations of the 1D model describing the Light-Fluid dynamics. Top: Numerical simulations of the experiments presented in (c), are in qualitative agreement with the experiments: exhibiting a dense shock front trailed by a particle-cleared volume. Bottom: Calculated shock profile along the channel at three successive times. The shock's concentration increases as it propagates and picks up ('sweeps') the nanoparticles from its path.

Interestingly, Figs. 2(a) and 2(b) reveal, in addition to the propagating shock fronts, the formation of a long needle-like directional filament propagating deep into the scattering medium, along the axis of the channel. Possibly, these filaments are formed by the optical gradient force pulling the high refractive index particles into the incoming beam, self-inducing a waveguide. This effect has been reported before in dilute suspensions [16,17], but not in heavily scattering liquid media. This self-guiding effect occurs slowly, and the filament builds itself from the fiber and into the suspension in a series of unstable events. This type of wave-guiding filaments may facilitate a way to insert directional, non-diffusive light deep into heavy scattering systems – allowing deep probing of such suspensions with non-diffusive light, a feature much desired in medical imaging.

We harness these effects driven by the optical forces to induce a suspension-to-gel phase transition in small, preselected volumes deep inside the light-scattering fluid. When the light-fluid waves are launched in the thin microfluidic channel that constrains their propagation to one dimension, (Fig. 2(b)) we observe particulate accumulation at the tip of the propagating spear-head shock-front. The geometric constraint restricts the propagation of the shock waves, and the stiff boundaries at the micro-channel walls force a flow pattern that re-circulates the nanoparticles into the light beam. The light beam, in turn, pushes these particles into a concentrated region at the tip of the spearhead shock, amplifying their rate of accumulation, and 'jamming' them together. This process is readily visible in "Media 2", "Media 3" and "Media 4" available online, and the particle– accumulation is shown in Figs. 2(b-iv), and 3(a). In Fig. 3(a) and "Media 3", when the laser beam is subsequently turned off, the concentrated region remains locked in place, and the concentration profile is effectively 'written' into the suspension. But this is where we observe another intriguing effect: light-induced phase transition into a gel. When a silica suspension is concentrated to ~20%, it typically undergoes a suspension-to-gel phase-transition, transforming from a liquid suspension to a viscous gel [9]. If the laser beam is strong enough and is kept on long enough, the concentration of the nanoparticles at the concentrated region increases to such high values so as jellification occurs. As the concentration of nanoparticles exceeds ~20%, a dense 'gel ball' forms, and it is trapped inside the central filament of light (Fig. 3(b)-left). In this case, when the laser beam is subsequently turned off, the concentrated region does not remain written in place (as in Fig. 3(a) and the movie "Media 3"), but rather drops down with gravity. This effect is clearly visible in (Fig. 3(b), right), and the formation process of the gel-ball following the light-induced phase-transition is also presented in "Media 4" available online. Keeping in mind that for silica nanoparticles in the liquid-suspension phase, gravitational forces are negligible in comparison to Brownian forces, this downward motion with gravity is only possible if the condensed gel-ball has macroscopic dimensions of ~10μm or more, as the density of silica is twice that of water. Indeed, as observed in Fig. 3(b), the size of the gel-ball is ~10-20µm. Depending on the material the nanoparticles are made of and on the experimental conditions, this gelation can be made reversible.
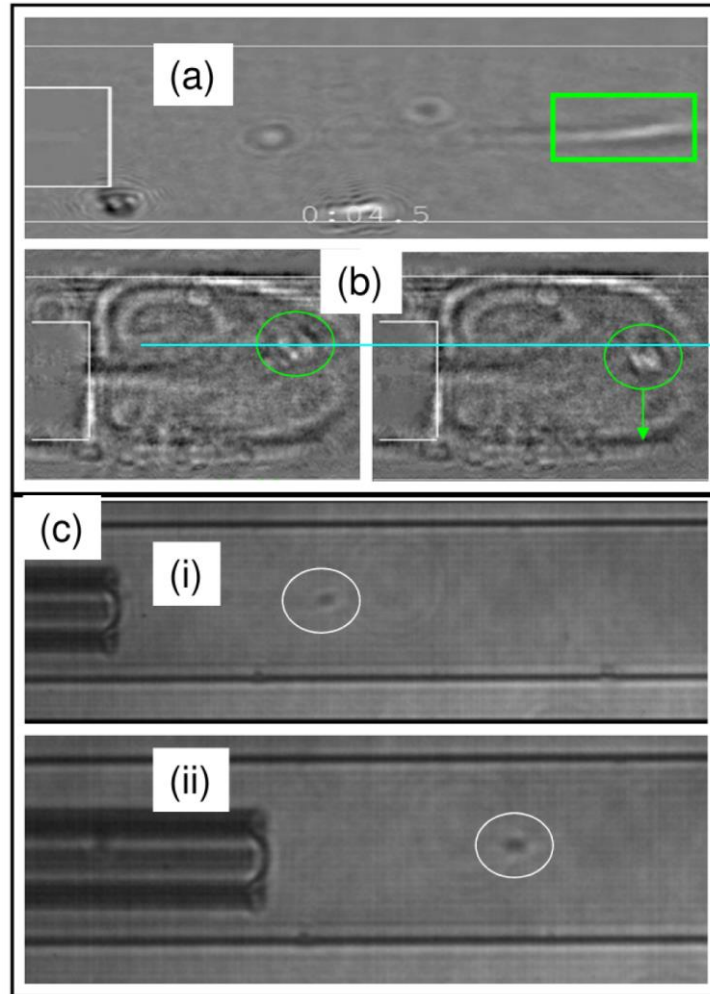
Fig. 3. Optical manipulation of the local properties of opaque scattering suspension. (a) Writing of a concentration spot. As the laser is switched on, a region of high nanoparticles accumulation (encompassed with green rectangle) is 'written' at the tip of the spearhead shock front. When the laser is turned off, the high concentration of nanoparticles remains 'written' in place, a distance of ~14 photon transport MFPs inside the suspension. This particle accumulation dissolves away slowly, on time scales of the particle diffusion in the suspension. This process is presented in 'Media 3' online. (b) Light-induced localized phase-transition inside light scattering suspension: Left: A shock wave propagates in a 10%, silica nanoparticle suspension. The light-induced concentration of nanoparticles at the accumulation point exceeds the critical concentration and transitions into a localized gel ball deep inside the opaque suspension. Right: Once the laser is turned off, the gel ball (marked in green circles) drops down with gravity, as apparent from comparing the left and right images. The cyan line is drawn to assist the visual comparison. This process is presented in 'Media 4' online (c) Optical manipulation of matter 'balls' deep inside light-diffusive suspensions. The laser is kept continuously on. An accumulation of polystyrene nanoparticles (encircled in white) develops ~6 transport MFPs to the right of the fiber. The nanoparticle accumulation is pushed to the right by radiation pressure as the fiber is moved between the two positions presented in the top and bottom images. This process is presented in 'Media 5' online.

Last, we demonstrate direct manipulation of matter deep inside the highly scattering suspension. We use a focused beam of light to generate dense gel balls several photon MFP's from the tip of an optical fiber inside a dense suspension filling a microfluidic channel. Such a

gel ball is subsequently positioned at a desired location inside the channel by moving the fiber itself. The ball is trapped inside the light-fluid filament for as long as the laser is on (Fig. 3(c)). Moving the fiber towards this sphere (to the right in Fig. 3(c)) places the object in a region where radiation pressure is nonezero. The pressure exerts force on the ball, moving the matter ball to the right. Figure 3(c) (top and bottom), shows the polystyrene ball at two locations, while "Media 5" available online displays the continuous manipulation of such matter ball – where we move the fiber and the ball follows the movement. Once the light is turned off, the nanoparticle accumulation resides in place, and it is in essence 'written' into the fluid, diffusing away on time scales of the particle diffusion, or slowly sinking with gravity. This type of effect, namely, laser- 'writing' of concentration profiles in 3D inside scattering suspensions may find applications in the growing industry of 3D printing.

4. Discussion

To our knowledge, the experiments present here are the first technique to ever work for manipulation in an opaque suspension. In what follows we discuss our work in the context of the available state of the art:

Recent advances in linear optic techniques allow focusing of light through turbid media using wavefront correction methods [10–13]. These methods hold the potential for revolutionizing biomedical imaging. However, these methods typically rely on feedback schemes: an optical wavefront shaped by a spatial-light modulator (SLM) is launched through scattering media, and the output light beam is collected by a camera, compared computationally to a desired focal spot, and electronic feedback is sent back to the SLM using some optimization algorithm, until an optimal focus is achieved. The need for a feedback loop makes these methods suitable to focus light layers of time-stationary scattering media. These methods can adapt to time variations in the scattering medium on the order of seconds [18] at best, making them completely unsuitable for suspensions of Brownian particles which move faster than the wavefront can adjust. Time-varying aberrations caused by the optical forces exerted by the manipulating light itself will probably cause additional complication. As such, to date these methods were not used for optical manipulation deep inside opaque suspensions.

In a similar vein, nonlinear interactions between light and fluids have been studied since Ashkin's pioneering experiments [16] in the early eighties. Various types of light induced liquid flows and patterns have been studied in scenarios ranging from optical forces acting of dilute colloid suspensions [16,17], polymer suspensions [19–21], critical microemulsions [22] and electrosctriction [23] to thermal interactions relying on heat diffusion and thermophoresis [24–27]. However, thus far these studies were carried out in optically-clear suspensions: suspensions that are dilute enough such that scattering can either be completely ignored, or at most treated as a 'single' scattering event. In contradistinction, this article demonstrates nonlinear light-fluid interactions in opaque suspensions, providing means to control the flow and the local properties of dense colloidal suspensions using light. Finally, recently it was shown that that light may induce superdiffusion in scattering suspensions [28], modifying the rate of a spatially global (non-local) linear process. In contrast, our work reveals that nonlinear light-fluid interactions in dense suspensions, rather than enhancing particle diffusion, result in anti-diffusive behaviors, such as localization and concentration of particles in moving shock fronts or small space-stationary volumes, filamentation, and local volume phase transition.

Counter to intuition, 'diffuse' light can be used to locally manipulate the local properties of light-diffusing fluids. We find these effects intriguing since to the naked eye, light entering these suspensions seems to diffuse in all directions without order, but in reality- rich localized and directional dynamics occur within the 'dazzling ball' of scattered light. Importantly, tailoring the deeply penetrating light-induced shock waves instead of the quickly diffusing optical field is a new approach, overcoming a fundamental limitation to optical manipulation. Interestingly, optical manipulation of dense scattering suspensions is far more efficient than

traditional tailoring of the optical field, since unlike in 'clear' suspensions, in opaque suspensions, diffusion of light ascertains that all of the momentum carried by light transfers to the particles and waves, which in turn do the manipulation. We can imagine more applications to come: light controlled chemical reactions inside dense colloid suspensions, where different reagents will be concentrated and manipulated to come to contact, transport and concentration of nanoparticle based drugs in moving shock fronts, manipulation, analysis and cleaning of opaque polluted fluids, and more. Not the least, the phenomena herein described, and specifically the light-induced gelation, may facilitate generation of interesting metastable glassy states- that are known to form under fast, far from equilibrium dynamics [29]. As such, we envision that the work presented here will open new frontiers for the rapidly evolving field of optofluidics: paving way to more research that will unravel the complexity of light-fluid coupled dynamics, and making optical control over the local properties of dense fluids in on-chip applications a reality.

Appendix

A. Derivation of the Burgers equation (Eq. (2) in the article)

Consider a beam of light having a time-averaged Poynting vector $<\vec{S}>$, illuminating a dielectric particle with scattering cross-section $\sigma_s(1-g)$. The anisotropy factor, g, accounts for the fraction of the optical power scattered in the same direction as $<\vec{S}>$, not transferring net momentum to the particle. It is a measure of the isotropy of the scattering profile. The pressure that light beam exerts on the particle in the direction of $<\vec{S}>$ is [30]:

$$P_{rad} = \frac{<\vec{S}>}{\tilde{c}}(\sigma_s(1-g)) = \frac{\hbar w \vec{J}^{ph}}{\tilde{c}}(\sigma_s(1-g)), \qquad (3)$$

where $\hbar$ is the plank constant divided by 2π, and $w, \tilde{c}, \vec{J}^{ph}$ are the frequency of light, the speed of light in the medium, and the photon flux, respectively. P_{rad} is henceforth referred to as the 'radiation pressure'.

Another component of pressure acting on the particle arises when the light illuminating the particle has a spatially non-uniform intensity. In that case, it exerts an 'optical-gradient force' [6] on the particle,

$$\vec{F}_{grad} = \frac{1}{2}\alpha\vec{\nabla}(E^2) = \frac{1}{2}\alpha\vec{\nabla}(I), \qquad (4)$$

where I is the light intensity, and α is the polarizability of the particle.

Noting that the light intensity is related to the time averaged photon density through $U = \frac{1}{2}\varepsilon_0 n^2 I = \hbar w \varphi_{ph}$, where φ_{ph} (w was stated above) is the photon density Eq. (4) can be rewritten as

$$\vec{F}_{grad} = \frac{1}{2}\alpha\vec{\nabla}(\frac{2\hbar w \varphi_{ph}}{\varepsilon_0 n^2}) = \frac{\alpha\hbar w}{\varepsilon_0 n^2}\vec{\nabla}\varphi_{ph} \qquad (5)$$

Suppose now that a liquid medium incorporates a concentration ρ (per unit volume) of dielectric particles. Light irradiates the medium. If the scattering is such that g<<1, meaning that most of the power is scattered isotropically, and - if the physical size of the system is much larger than the average distance a photon travels between scattering events (the photon transport mean free path, l_t), light can be thought of as exercising a 'random walk' between

the particles [8], where the random arrangement of the particles is responsible for the randomness of the 'walk'. In this case, the photon flux $\vec{J}^{ph}$ can be approximated by the continuity equation along with Fick's law of linear transport [7],

$$\frac{\partial \varphi_{ph}}{\partial t} + \vec{\nabla} \cdot \vec{J}^{ph} = 0 \, ; \, \vec{J}^{ph} = -D_{ph} \vec{\nabla} \varphi_{ph}, \qquad (6)$$

where D_{ph} is the diffusion coefficient for photons, and $\vec{J}_{ph}$ their flux. Rearranging Eq. (6) results in a diffusion equation for φ_{ph},

$$\frac{\partial \varphi_{ph}}{\partial t} = \vec{\nabla} \cdot \left(D_{ph} \vec{\nabla} \varphi_{ph} \right). \qquad (7)$$

The photon diffusion coefficient, D_{ph}, can be expressed in terms of the transport MFP length as

$$D_{ph} = \frac{\tilde{c} l_t}{3} \qquad (8)$$

with

$$l_t = \frac{1}{\left[\sigma_s \left(1 - g \right) \right] \rho} \qquad (9)$$

in lossless media. From (7-9), we formulate one equation for ρ, φ_{ph}:

$$\frac{\partial \varphi_{ph}}{\partial t} = \vec{\nabla} \cdot \left(\frac{\tilde{c}}{3 \left[\sigma_s \left(1 - g \right) \right] \rho} \vec{\nabla} \varphi_{ph} \right). \qquad (10)$$

In a solid, ρ is a constant quantity, and Eq. (10) is a linear diffusion equation. In a fluid, however, the particle density ρ in Eq. (10) is a dynamic quantity - that is, it does not remain uniform in space and time: the same light that scatters from the particles also exerts optical forces on the scattering particles, changing their initially uniform distribution in the fluid.

With respect to the condition g<<1, we note that the 100nm Polystyrene particulate suspension and the 150nm Silica particle suspension support this assumption well, whereas the 320nm Silica suspension shown in Fig. 3(b) does not. Evidently, although nonlinear light-induced shocks can be observed in the latter suspension too, its theoretical description is beyond the scope of the present work.

To account for the possible motion of the particles, we introduce a linear transport equation for ρ under the influence of radiation pressure, the optical gradient forces, and particle diffusion (with diffusion coefficient D_{par}). Continuity requires that,

$$\frac{\partial \rho}{\partial t} = \vec{\nabla} \cdot \left(D_{par} \nabla \rho - \mu \rho \left(\vec{F}_{rad} + \vec{F}_{grad} \right) \right), \qquad (11)$$

where the terms in parenthesis on the right hand side of (11) are just the particle flux, and μ is the mobility of the particles.

We substitute the optical forces from Eqs. (3-5) into Eq. (11): We replace $\vec{F}_{rad}$ with Eq. (3), and substitute $\vec{J}_{ph}$ with $\left(-\dfrac{v}{3\left[\sigma_s \left(1-g \right) \right] \rho} \nabla \varphi_{ph} \right)$ as in Eq. (10). For the gradient force, we substitute Eq. (5). The result is an equation for ρ,

$$\frac{\partial \rho}{\partial t} = \vec{\nabla} \cdot \left(D_{par} \nabla \rho + \rho \mu \left(\frac{\hbar w}{3\left[\sigma_s \left(1-g \right) \right] \rho} \nabla \varphi_{ph} \left[\sigma_s \left(1-g \right) \right] \right) + \frac{\alpha \hbar w}{\varepsilon_0 n^2} \nabla \varphi_{ph} \right) =$$

$$= \vec{\nabla} \cdot \left(D_{par} \nabla \rho + \frac{\mu \hbar w}{3} \nabla \varphi_{ph} \left(1 - \frac{3\alpha \rho}{\varepsilon_0 n^2} \right) \right) \tag{12}$$

We assume that the photon density always reaches a steady state much faster that the particle concentration. This assumption is justified by comparison of the diffusion times of the photons and the particles:

$$\frac{t_{par}}{t_{ph}} = \frac{D_{ph}}{D_{par}} = \frac{\tilde{c}}{3\left[\sigma_s \left(1-g \right) \right] \rho} \frac{T}{6\pi \eta a} \tag{13}$$

where in the last equality we take advantage of the Einstein-Stokes relation, and η is the viscosity of the liquid. Taking for example $l_t = 100 \mu m$, $\eta \sim 10^{-3} Pa \cdot \sec$ and $T = \sim 4 \cdot 10^{-21} J$ at room temperature, and a 1μm particle, we have $\dfrac{t_{par}}{t_{ph}} \cong 10^{-9}$, justifying the above assumption.

Accordingly, Eq. (10) for the continuity of photon flux becomes time-independent.

Considering a 1D geometry, Eq. (10) simplifies to $0 = \dfrac{\partial}{\partial x} \cdot \left(\dfrac{\tilde{c}}{3\left[\sigma_s \left(1-g \right) \right] \rho} \dfrac{\partial}{\partial x} \varphi_{ph} \right)$, whose solution is

$$\frac{\partial}{\partial x} \varphi_{ph} = C \frac{3\left[\sigma_s \left(1-g \right) \right] \rho}{\tilde{c}} \triangleq C_1 \rho, \tag{14}$$

where C, C_1 are constants. Introducing (14) into (12), we have

$$\frac{\partial \rho}{\partial t} = \frac{\partial}{\partial x} \cdot \left(D_{par} \rho_x + \frac{\mu \hbar w}{3} \left(1 - \frac{3\alpha \rho}{\varepsilon_0 n^2} \right) C_1 \rho \right) = D_{par} \rho_{xx} + \frac{\mu \hbar w}{3} C_1 \rho_x - \mu \hbar w \frac{2\alpha \rho \rho_x}{\varepsilon_0 n^2} C_1 =$$

$$= D_{par} \rho_{xx} + \frac{\mu \hbar w}{3} C_1 \rho_x \left[1 - \frac{6\alpha \rho}{\varepsilon_0 n^2} \right] \triangleq D_{par} \rho_{xx} + A\rho_x - B\rho \rho_x \tag{15a}$$

where in Eq. (15a) and hence on, we use $\dfrac{\partial}{\partial x} \leftrightarrow \partial_x$ interchangeably.

Eq. (15a) is a nonlinear equation for ρ. It can be transformed to the form of the Burger's equation, using the transformation

$$X = x + At$$
$$t = \tau \tag{15b}$$

We rewrite Eq. (15) in form of the Burger's equation,

$$\rho_\tau + A\rho_X = D_{par}\rho_{XX} + A\rho_X - B\rho\rho_X \tag{16}$$

which is just

$$\rho_\tau = D_{par}\rho_{XX} - B\rho\rho_X \tag{17}$$

We note that the Burger's equation[5] is now in a frame of reference moving with velocity $A = \dfrac{\mu\hbar w}{3}C_1$. To find the constant A for the transformation we use Eq. (14), $\dfrac{1}{\rho}\dfrac{\partial\varphi_{ph}}{\partial x} = C_1$,

and utilize $\bar{J}^{ph} = -\dfrac{\tilde{c}}{3\sigma_s(1-g)\rho}\dfrac{\partial\varphi_{ph}}{\partial x} = <S>/\hbar w$ from Eq. (10) to get

$$C_1 = \frac{1}{\rho}\frac{\partial\varphi_{ph}}{\partial x} = \frac{<S>}{\hbar w\tilde{c}}3\sigma_s(1-g) = \frac{3P_{rad}}{\hbar w}. \tag{18}$$

Introducing the last result into the velocity A, and using Eq. (3):

$$A = \mu\frac{<S>}{\tilde{c}}\sigma_s(1-g) = \mu P_{rad} \tag{19}$$

In a system with particle Reynolds number<<1, the velocity A for the transformation of coordinates Eqs. (15a-15b), is just the drag velocity of the particle at the plane in which lightnters the system, since

$$v_{drag} = \mu P_{rad} = \frac{P_{rad}}{6\pi\eta a}, \text{ and accordingly, } C_1 = \frac{3v_{drag}}{\mu\hbar w}.$$

To summarize this section, we introduce the constant C_1 into Eq. (17), to arrive at the equation governing the nanoparticle dynamics in the system:

$$\frac{\partial\rho}{\partial\tau} = D_{par}\rho_{XX} - \rho_X\rho\frac{6\alpha v_{drag}}{\varepsilon_0 n^2} \tag{20}$$

In a 1D system, if a beam of light is launched into the system of strongly scattering particles, the equation for the time-dependent distribution of nanoparticles is the Burgers equation [15] - Eq. (20) above, which describes shock waves in a frame of reference moving at the drag velocity that the radiation pressure dictates. Equation (2) in the article is in the same form of Eq. (20), but here the constants are written explicitly as functions of the relevant physical quantities. Notably, the Burger's Eq. (20) supports shock wave solutions.

B. Ruling out thermal effects in the experiments.

The absorption of green light by silica and polystyrene is negligible over the dimensions of the channel. The absorption coefficients are $\mu_a \sim 10^{-7}cm^{-1}$ and $\mu_a < 10^{-4}cm^{-1}$, for silica [30] and polystyrene [31] respectively. Theoretically, the effects shown in the Article should have close to no thermal involvement at all. However, to ascertain this assumption and make sure the effects we report involve no thermal origin, we characterized the materials and the components of the experimental setup using a commercial thermal camera (Electro-optics EzTherm®). The resolution of the camera is ~1°F). Below we describe this set of experiments. The materials used in the experiments are the same as those used in the shockwave-generation experiments reported in this this Article, and are listed below:

1.Silica 150nm spheres in water, 10% w/v, obtained from 'Bangs laboratories'.

2.Silica 320nm spheres in water, 10% w/v, obtained from 'Bangs laboratories'.

3.Silica 390nm spheres in water, 10% w/v, obtained from 'Bangs laboratories'.

4.Polystyrene 100nm spheres in water, 10% w/v, obtained from 'Bangs laboratories'.

5.Polystyrene 200nm spheres in water, 10% w/v, obtained from 'Bangs laboratories'.

In a first set of experiments, for each of these materials, two small droplets (10 μliter each) are put on a glass microscope slide. A laser beam with power ranging 1-8 watts illuminated one of the droplets continuously, for periods up to 2 minutes, while the other droplet was used as control. The droplets were imaged continuously with a thermal camera, and images of the droplets were recorded before and immediately at the end of illumination for each measurement.

In a second set of experiments, the same optic fiber used in the experiments shown in the Article was dipped in the droplets, and 3 watts of green light were coupled into the droplet through the fiber. A thermal image of the droplets+Fiber was taken before and immediately at the end of illumination for each measurement.

In a third set of experiments, the fiber was dipped into the suspension. When it was subsequently raised from the droplet, a small drop of liquid accumulated at the fiber tip's end. The volume of this droplet was much smaller than 10μliter. The laser was subsequently turned on- and the tip of the fiber was imaged with the thermal camera.

In all of the experiments, the illuminated droplet showed negligible temperature difference ($\leq 1°F$). An example of such results is shown in Fig 4. Keeping in mind that the suspensions were illuminated in these experiments up to 3 times more intensely and up to 12 times longer than the suspensions in the shockwave generation experiments in the Article, we conclude that there is no thermal involvement in the effects this Article reports.
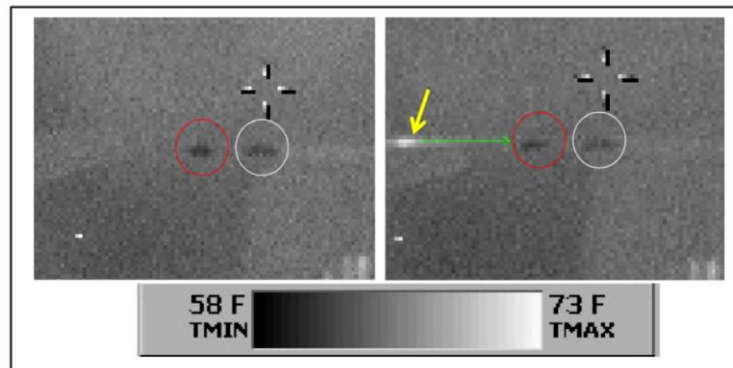

Fig. 4. Left: Two drops of nanoparticle suspension (silica, 10%, 150nm, encircled in red and in white) are imaged with a thermal camera. Right: A fiber (invisible with the resolution of the camera, and marked with a green arrow) is inserted into the droplet marked in red. Green laser light couples into the fiber, and is continuously applied to the droplet for one minute. Evidently, the droplet does not heat up, as it remains at the same temperature as the control droplet (encircled in white). For comparison, note that the fiber is supported on a steel stand (marked with a yellow arrow), and slight leakage of light from the fiber to this stand heats it up significantly. The 'target cross-hair' mark in the images is a feature of the camera and has no special meaning in the context of this figure.

C. Setup for interferometric measurements.

The setup used for characterizing the density profile of the shock-fronts is depicted in Fig. 5. A near infra-red (NIR) plane wave (broadened Gaussian beam) is split into orthogonal polarizations (marked in red and blue in the figure). One polarization if used to illuminate the

channel from the side with a plane wave, facilitating regular fast imaging such as in Fig. 2(a), 2(b) in the Article, or in Media 1 and Media 2 online. The other beam is again split to two. One part of the beam is used as reference arm for the interferometer, and the other is focused into the channel through its glass wall- to ~5 μm spot. This is the interferometer probe beam. The probe beam exits through the wall on the other side of the glass cell, and is subsequently re-collimated using an objective lens. The collimated beam interferes with the reference beam, to yield a zero-order fringe. Slight (deliberate) misalignment allows the beams to form an interference fringe pattern such as the one shown in Fig. 5. When the shock-front propagates through the channel, it introduces a phase change to the probe beam, which translates directly to a motion of the fringe pattern. Measuring the dynamics in the channel simultaneously with the interferometric signal, we see that as the shock front approaches and crosses the location of the probe beam, the fringes start to move. Measuring the fringe motion as a function of time, we record the phase change that the probe beam undergoes as a function of time. The change in the phase that the probe beam accumulates as the shock front passes through it is

$$\delta\phi(t) = \frac{2\pi \cdot \delta n(t) \cdot W}{\lambda} \qquad , \tag{21}$$

where W and λ are the width of the channel and the wavelength, and $\delta n(t)$ is the time-dependent refractive index change, which is due to a change in the composition of the suspension at the path of the beam. The composition of the suspension is different from the bulk suspension, because the nanoparticles concentrate the shock front. Suppose that the concentration of nanoparticles in the bulk is C_0, then at the shock front passing through the probe beam at time t, the concentration of nanoparticles is denoted $C_0 + \delta c(t)$. Denoting the difference between the refractive indices of the suspended particles and the water β, $\delta n(t) = \beta \cdot \delta c(t)$. Values of β are, for examples, 0.12 and 0.26 for our silica and polystyrene suspensions respectively. Finally,

$$\delta\phi(t) = \frac{2\pi \cdot \beta \cdot \delta c(t) \cdot W}{\lambda} \tag{22}$$

The optical path on which the optical phase accumulates was taken as W in Eqs. (21-22), but a better estimate can be extracted directly from the simultaneous imaging of the dynamics. Hence it is possible to replace W in Eqs. (21-22) with the width of the observed shock fronts. In the measurements presented in Fig. 2b in the Article, W was replaced with 50μm. The time dependent phase $\delta\phi(t)$ is measured from the fringe motion with a fast (~200 fps) camera, and $\delta c(t)$, the concentration at the shock-front, is extracted using Eq. (22).
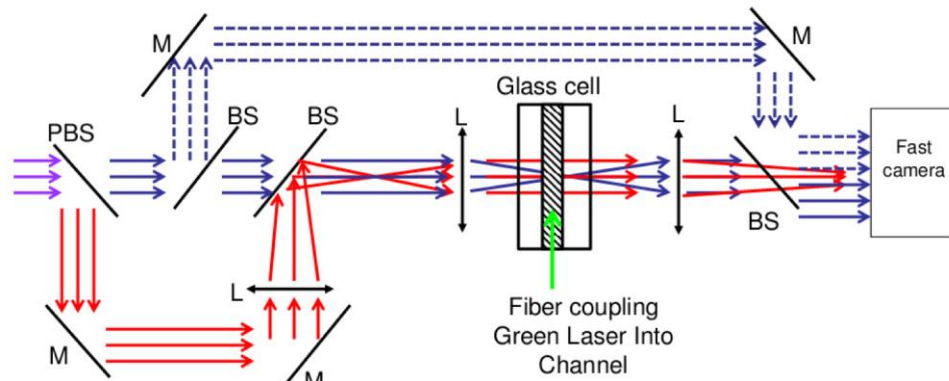
Fig. 5. Schematic of the interferometric setup (not to scale, arrows illustrate ray trajectories but are not precise ray traces). A NIR beam (purple arrows) is split into two orthogonal polarizations. One polarization (red arrows) facilitates direct imaging (shadowgraphy) of the dynamics in the channel. The other polarization is also split into two: one part (blue whole arrows) is focused into the fluid channel, where it is used as a probe of nanoparticle concentration changes, as a shockfront crosses its path. This beam is subsequently collimated, and is interfered with a reference beam of the same polarization (blue dashed arrows) on the sensor of a fast camera (~200fps). The resulting interference signal is recorded in real time simultaneously with the imaged dynamics, and analyzed offline. The shock-front is generated in the channel using green CW laser light which is coupled to the channel through the fiber. In the drawing: L = Lens, M = Mirror, BS = beam splitter, PBS = Polarizing beam splitter.

Acknowledgments